Direct Synthesis and Solid-State NMR Characterization of Cubic Mesoporous Silica SBA-1 Functionalized with Phenyl Groups

Hsien-Ming Kao,*,† Chia-Hsiu Liao,† Tzu-Ti Hung,† Yu-Chi Pan,† and Anthony S. T. Chiang‡

Department of Chemistry and Department of Chemical and Materials Engineering, National Central University, Chung-Li, Taiwan 32054, R.O.C.

Received January 15, 2008

Well-ordered mesoporous silicas SBA-1 (cubic *Pm*3*n* symmetry) functionalized with phenyl groups have been synthesized via co-condensation of tetraethoxysilane (TEOS) and phenyltriethoxysilane (PhTES) under acidic conditions. The synthesis parameters such as temperature, type of surfactant, and synthesis composition have been systematically investigated as a function of PhTES contents. The phenyl-containing units are incorporated quantitatively and reach a maximum PhTES loading up to 33 mol % (based on silicon) without a significant degradation of the structural ordering of the *Pm*3*n* mesophase. A combination of multinuclear (^{1}H, ^{13}C, ^{29}Si) solid-state NMR and two-dimensional (2D) solid-state NMR correlation techniques such as ^{13}C{^{1}H} and ^{29}Si{^{1}H} HETCOR (heteronuclear correlation) and ^{1}H-^{1}H exchange NMR has been used to establish framework locations of phenyl functional groups that are incorporated in the mesoporous structure and their interactions with the surfactant molecules. 2D ^{13}C{^{1}H} HETCOR NMR experiments reveal that the phenyl moieties are in close spatial proximity to the trimethylammonium headgroups of the cationic surfactant species in the as-synthesized materials, suggesting that there are some specific interactions between them to maintain the surfactant packing parameter (g) smaller than 1/3 necessary for the formation of the cubic mesophase. The detection of couplings between the protons associated with various ^{29}Si species via ^{29}Si{^{1}H} HETCOR NMR established that the T silicon species due to the phenyl groups incorporated are in closer proximity to the Q^4 silicon species than to the Q^3 silicon species. This observation also provides direct molecular-level evidence for the co-condensation of PhTES and TEOS in the synthesis of mesoporous organosilicas.

Introduction

Since the first report on the surfactant templated synthesis of the ordered M41S family of mesoporous materials,[1] much research has been devoted to studies on the modification, fabrication and application of ordered mesoporous materials. Of particular current interest is functionalization of mesoporous materials via organic modifications. These mesoporous organosilica materials possess well-defined pore structures, highly accessible functional groups, and controlled surface reactivity[2–15] and therefore open a new opportunity to tune the materials for specific uses in the fields of catalysis, sensing, and adsorption. The so-called "direct synthesis" method is based on co-condensation of organotrialkoxysilane with another silicon source, such as tetraethoxysilane (TEOS) using surfactants as structure-directing agents to prepare ordered mesoporous silicas with high loadings of pendant organic groups. This synthesis route is often preferred to the postsynthesis grafting because it offers a higher loading and a more uniform distribution of organic functional groups without closing the framework mesopores.[11] While some of these materials were well ordered, most of the previously reported co-condensation methods resulted in breakup of the structural integrity and long-range periodicity at surface coverages exceeding 20%; at higher ratios poorly ordered products were often obtained. Furthermore, the organic functions may not be necessarily all located at the pore surface, especially for high loadings of functional groups.

Functionalization of mesoporous materials with cubic symmetry has received relatively little attention as compared to those with hexagonal symmetry such as MCM-41 and SBA-15. Huo et al.[16–18] reported the synthesis of a cage-

* Corresponding author. Tel.: +886-3-4275054. Fax: +886-3-4227664. E-mail: hmkao@cc.ncu.edu.tw.
† Department of Chemistry.
‡ Department of Chemical and Materials Engineering.

(1) Kresge, C. T.; Leonowicz, M. E.; Roth, W. J.; Vartuli, J. C.; Beck, J. S. *Nature* **1992**, *359*, 710.
(2) Burkett, S. L.; Sims, S. D.; Mann, S. *Chem. Commun.* **1996**, 1367.
(3) Macquarrie, D. J. *Chem. Commun.* **1996**, 1961.
(4) Macquarrie, D. J.; Jackson, D. B. *Chem. Commun.* **1997**, 1781.
(5) Lim, M. H.; Blanford, C. F.; Stein, A. *J. Am. Chem. Soc.* **1997**, *119*, 4090.
(6) Fower, C. E.; Burkett, S. L.; Mann, S. *Chem. Commun.* **1997**, 1769.
(7) Lim, M. H.; Blanford, C. F.; Stein, A. *Chem. Mater.* **1998**, *10*, 467.
(8) Moller, K.; Bein, T.; Fischer, R. X. *Chem. Mater.* **1999**, *11*, 665.
(9) Stein, A.; Melde, B. J.; Schroden, R. C. *Adv. Mater.* **2000**, *12*, 1403.
(10) Sayari, A.; Hamoudi, S. *Chem. Mater.* **2001**, *13*, 3151.
(11) Lim, M. H.; Stein, A. *Chem. Mater.* **1999**, *11*, 3285.
(12) Asefa, T.; Kruk, M.; MacLachlan, M. J.; Coombs, N.; Grondey, H.; Jaroniec, M.; Ozin, G. A. *Adv. Funct. Mater.* **2001**, *11*, 447.
(13) Kruk, M.; Asefa, T.; Jaroniec, M.; Ozin, G. A. *J. Am. Chem. Soc.* **2002**, *124*, 6383.
(14) Mercier, L.; Pinnavaia, T. J. *Chem. Mater.* **2000**, *12*, 188.
(15) Babonneau, F.; Leite, L.; Fontlupt, S. *J. Mater. Chem.* **1999**, *9*, 175.
(16) Huo, Q.; Margolese, D. I.; Ciesla, U.; Demuth, D. G.; Feng, P.; Gier, T. E.; Sieger, P.; Firouzi, A.; Chmelka, B. F.; Schüth, F.; Stucky, G. D. *Chem. Mater.* **1994**, *6*, 1176.
(17) Huo, Q.; Leon, R.; Petroff, P. M.; Stucky, G. D. *Science* **1995**, *268*, 1324.
(18) Huo, Q.; Margolese, D. I.; Stucky, G. D. *Chem. Mater.* **1996**, *8*, 1147.

10.1021/cm800147z CCC: $40.75
Published on Web 03/05/2008

like cubic mesoporous molecular sieve denoted SBA-1 (cubic *Pm*3*n*) through the $S^+X^-I^+$ pathway, where S, X, and I correspond to surfactant, halide, and inorganic species, respectively, by implementation of strongly acidic conditions and surfactants with large headgroups such as cetyltriethylammonium bromide (CTEABr). Up to now, however, surprisingly little research has been reported on the direct synthesis of organo-functionalized SBA-1. This can be attributed in part to tits low synthesis temperature conditions, resulting in the poor stability of as-synthesized SBA-1 toward washing with water.[19–21] This stability problem imposes some limitations on the direct incorporation of organic functionality into SBA-1 since surfactant removal often needs solvent extraction treatment. Moreover, the large headgroup surfactant CTEABr used for the conventional synthesis of SBA-1 is not commercially available. We have first reported a successful synthesis of the SBA-1 mesostructure functionalized with vinyl groups under strongly acidic conditions templated with CTEABr.[22]

The organic functional groups introduced by organotrialkylsilane may play an important role in the self-assembly mechanism. For example, Goletto et al.[23] reported the direct incorporation of phenyl groups into the *Pm*3*n* structure in acidic media using cetyltrimethylammonium bromide (CTMABr) as the surfactant. For the formation of the cubic *Pm*3*n* mesophase, the surfactant micellar structure requires large surface curvature and low charge density. As a result, their formation is favored by the use of surfactant molecules with large polar headgroups like CTEABr, and acidic conditions under the charge density at the silicate−surfactant interfaces are always limited. It should be noted that the material templated with CTMABr often leads to a hexagonal SBA-3 mesophase under acidic conditions when TEOS is used as the only silicon source. The incorporation of phenyl groups via phenyltriethoxysilane (PhTES) makes the formation of the SBA-1 mesostructure possible, suggesting the presence of some specific interactions between the phenyl groups and the polar headgroup of the surfactant molecules.[23] However, the cubic *Pm*3*n* structure was only obtainable at a TEOS: PhTES ratio of 4:1. Either hexagonal or mixed phases were formed with other TEOS/PhTES ratios.[24] This is a very unusual case for the preparation of mesoporous organosilicas. In general, the structural ordering of a given mesophase is progressively degraded as the concentration of the organic functional group incorporated is increased. Therefore, the synthesis conditions such as temperature and loading of phenyl groups and the interaction between the phenyl groups and the surfactant chains deserves more detailed investigation.

Although the structural properties in self-assembled mesophase materials have been well characterized, relatively few studies have been focused on a detailed characterization of the interactions that develop between the inorganic species and the structure-directing agents. These interactions are crucial to drive the self-assembly process and to produce variations in the structural properties of the final mesoporous materials. Thus, it is of great importance to use appropriate characterization tools not only to identify and quantify the building units but also most importantly to probe their spatial proximities and their interactions with the structure-directing agents. A powerful technique to provide detailed structural information regarding molecular and interfacial environments is solid-state NMR spectroscopy. This is often achieved with heteronuclear correlation (HETCOR) NMR spectroscopy by correlating the chemical shift of protons in the materials with the nearby ^{13}C or ^{29}Si species via their respective heteronuclear dipole–dipole couplings.[25–29] Such couplings depend strongly on the respective mobilities and separations of the nuclei involved, which allows the spatial proximities between the protons of the templating molecules and the selected nuclei present at the pore surface to be probed. However, investigations that focused on the relative spatial arrangement of the surfactant molecules with respect to the mesoporous organosilica framework are quite limited since most of the solid-state NMR characterization concerns the mesoporous materials after template removal. Recently, these 2D heteronuclear correlation experiments have been successfully applied to mesoporous materials functionalized with vinyl groups.[30,31] For the case of phenyl-functionalized mesoporous materials, the framework locations of the phenyl silicon species must be determined by their correlation to the surfactant as well as to the silica framework. 2D $^{13}C\{^1H\}$ and $^{29}Si\{^1H\}$ HETCOR NMR experiments will be advantageous to examine the molecular interactions that form the basis of the self-assembled structures.

It has been recognized that the content of organic groups is a key factor that determines many important properties of the hybrid materials, such as adsorption capacity for metal ions, enhanced hydrothermal stability, and surface reactivity

(19) Kim, M. J.; Ryoo, R. *Chem. Mater.* **1999**, *11*, 487.
(20) Vinu, A.; Murugesan, V.; Hartmann, M. *Chem. Mater.* **2003**, *15*, 1385.
(21) Kao, H.-M.; Ting, C. -C.; Chiang, A. S. T.; Teng, C. -C.; Chen, C. -H. *Chem. Commun.* **2005**, 1058.
(22) Kao, H.-M.; Wu, J.-D.; Cheng, C.-C. *Microporous Mesoporous Mater.* **2006**, *88*, 319.
(23) Goletto, V.; Dagry, V.; Babonneau, F. *Mater. Res. Soc. Symp. Proc.* **1999**, *576*, 229.
(24) Goletto, V.; Imperor, M.; Babonneau, F. *Nanoporous Materials II*; Studies in Surface Science and Catalysis 129; Sayari, A., Jaroniec, M., Pinnavaia, T. J., Eds.; Elsevier: Amsterdam, The Netherlands, 2000; p 287.
(25) Vega, A. J. *J. Am. Chem. Soc.* **1988**, *110*, 1049.
(26) Janicke, M. T.; Landry, C. C.; Christiansen, S. C.; Kumar, D.; Stucky, G. D.; Chmelka, B. F. *J. Am. Chem. Soc.* **1998**, *120*, 6940.
(27) Melosh, N. A.; Lipic, P.; Bates, F. S.; Wudl, F.; Stucky, G. D.; Fredrickson, G. H.; Chmelka, B. F. *Macromolecules* **1999**, *32*, 4332.
(28) Christiansen, S. C.; Zhao, D.; Janicke, M. T.; Landry, C. C.; Stucky, G. D.; Chmelka, B. F. *J. Am. Chem. Soc.* **2001**, *123*, 4519.
(29) Baccile, N.; Laurent, G.; Bonhomme, C.; Innocenzi, P.; Babonneau, F. *Chem. Mater.* **2007**, *19*, 1343.
(30) Trébosc, J.; Wiench, J. W.; Huh, S.; Lin, V. S.-Y.; Pruski, M. *J. Am. Chem. Soc.* **2005**, *127*, 3057.
(31) Kao, H.-M.; Wu, J.-D.; Cheng, C.-C *Microporous Mesoporous Mater.* **2006**, *97*, 9.
(32) Delattre, L.; Babonneau, F. *Mater. Res. Soc. Symp. Proc.* **1994**, *346*, 365.
(33) Goletto, V.; Imperor, M.; Babonneau, F. *Zeolites and Mesoporous Materials at the Dawn of the 21st Century*; Studies in Surface Science and Catalysis 135; Galarneau, A., Di Renzo, F., Fajula, F., Vedrine, J., Eds.; Elsevier: Amsterdam, The Netherlands, 2001; p 1129.
(34) (a) Babonneau, F.; Bonhomme, C.; Gervais, C.; Maquet, J. *J. Sol-Gel Sci. Technol.* **2004**, *31*, 9. (b) Camus, L.; Goletto, V.; Maquet, J.; Gervais, C.; Bonhomme, C.; Babonneau, F. *J. Sol-Gel Sci. Technol.* **2003**, *26*, 311.
(35) Bronnimann, C. E.; Ziegler, R. C.; Maciel, G. E. *J. Am. Chem. Soc.* **1988**, *110*, 2023.
(36) Bronnimann, C. E.; Chuang, I.-S.; Hawkins, B. L.; Maciel, G. E. *J. Am. Chem. Soc.* **1987**, *109*, 1562.
(37) Hwang, S.-J.; Uner, D. O.; King, T. S.; Pruski, M.; Gerstein, B. C. *J. Phys. Chem.* **1995**, *99*, 3697.

and hydrophobicity. Therefore, there is a need to explore the achievable high loadings of the phenyl groups in the mesoporous silicas which are synthesized under acidic conditions. Because the previously reported results for SBA-1 functionalized with phenyl groups were rather unusual, this prompted us to perform a more detailed investigation on the synthesis parameters, such as synthesis temperature, type of the surfactant, and change in the composition, for the formation of the phenyl-functionalized SBA-1 mesostructure. This paper also highlights the use of two-dimensional solid-state NMR correlation techniques, including $^{13}C\{^1H\}$ and $^{29}Si\{^1H\}$ HETCOR and ^1H-^1H exchange NMR experiments performed on both as-synthesized and template-extracted materials to gain more insights in the framework location of phenyl functional groups and their specific interaction with the surfactant molecules.

Experimental Section

Materials Synthesis. Method A. Phenyl-functionalized SBA-1 was prepared via co-condensation of phenyltriethoxysilane (PhTES, from Aldrich) and a conventional silicon source TEOS (Aldrich). The synthesis procedure described earlier was slightly modified.[23,24] In a typical synthesis, TEOS and PhTES, with a molar ratio systematically varied from 9:1 to 1:1, were premixed and added to an aqueous HCl solution containing the surfactant CTMABr to obtain a homogeneous solution. After dissolution, the reaction was then continued at different synthesis temperature (0, 25, or 50 °C) under vigorous stirring for 4 h. Thereafter, the reaction mixture was then hydrothermally treated at 100 °C for 1 h. The resultant white precipitates were filtered, washed, and then dried at 60 °C overnight. The molar composition of the reaction mixture was 0.12 CTMABr:1 (TEOS + PhTES):9.2 HCl:130 H_2O. The materials obtained were denoted as A-Ph-MB/*x*, where *x* is the molar ratio of TEOS/PhTES and MB stands for CTMABr. Different surfactants such as CTMACl and CTEABr were also used, and the resulting samples were designated as A-Ph-MC/*x* and A-Ph-EB/*x*, respectively. The surfactant CTEABr was synthesized by following a previously published procedure.[16] It should be noted that the materials prepared in ref 23 were synthesized at ambient temperature and the two silicon precursors were not premixed for the method that can produce cubic *Pm*3*n* mesophase. When the two silicon precursors were prehydrolyzed in ethanol, a hexagonal mesophase was formed instead.[24]

Method B. The second series of samples were prepared at 0 °C according to the conventional composition for the synthesis of SBA-1,[19–21] that is, 0.2 surfactant:1 (TEOS + PhTES):46 HCl: 700 H_2O, and the resulting samples were designated as B-Ph-Z/*x*, where Z represents the surfactant and can be either MB, MC, or EB.

The template was removed from the material by a solvent extraction process, although calcination techniques can be also applied to the present special case due to the high thermal stability of Si−Ph bonds.[15,23] A suspension of 0.5 g of as-synthesized sample was stirred in a solution of 5 g of HCl (36 wt %) in 150 mL of ethanol at 50 °C for 3 h. The same procedure was repeated one more time.

Solid-State NMR Spectroscopy. Multinuclear (^1H, ^{13}C, ^{29}Si) solid-state NMR spectra were recorded on a Varian Infinityplus-500 NMR spectrometer, equipped with a 5 or 4 mm Chemagnetics probe. The Larmor frequencies for ^1H, ^{13}C, and ^{29}Si nuclei are 498.54, 125.37, and 99.04 MHz, respectively. Both ^{13}C and ^{29}Si CPMAS (cross-polarization magic angle spinning) NMR spectra were recorded by using a contact time of 1 ms and a recycle delay of 5 s. The ^{29}Si spin–lattice relaxation times in the mesoporous organosilicas were found to be in the range of 30 to 65 s.[32–38] Therefore, a $\pi/4$ pulse of 4 μs and a recycle delay of 400 s were used to acquire the quantitative ^{29}Si MAS NMR spectra. Deconvolution of the ^{29}Si MAS NMR spectra was performed with the PEAKFIT software.[39] The ^1H, ^{13}C, and ^{29}Si chemical shifts were externally referenced to tetramethylsilane (TMS) at 0.0 ppm.

The two-dimensional HETCOR NMR is similar to a standard CPMAS experiment. The pulse sequence consists of an initial time period (t_1) during which ^1H magnetization evolves freely without homonuclear ^1H-^1H decoupling, followed by a CP step with a contact time ranging from 1 to 5 ms that transfers polarization to dipolar-coupled ^{13}C and ^{29}Si spins, respectively, which are detected under high-power proton decoupling (r.f. strength $\nu_1 = 65$ kHz) during t_2. This experiment has been performed for ^1H-^{29}Si correlation studies of silanol groups in silicas and zeolites.[25] phase-sensitive detection was accomplished by using time-proportional phase incrementation (TPPI) phase cycling.[40] Fourier transformation in both time domains allows correlations to be made between the various proton species and the spatially proximate ^{13}C or ^{29}Si nuclei.

The 2D ^1H-^1H exchange NMR experiments were performed with a NOESY-type sequence with three 90° pulses. After the initial excitation, an additional $\pi/2$ pulse is incorporated after the evolution time (t_1) to store the ^1H magnetization along the *z*-axis, followed by a mixing time (t_{mix}), during which proton spin diffusion can occur. Magnetization is exchanged only between homonuclear dipolar-coupled proton species, and their separation can be probed by varying the mixing time. The ^1H-^1H exchange sequence produces homonuclear correlated spectra giving rise to off-diagonal intensities at positions where nuclei undergo chemical exchange or spin diffusion during the mixing time t_{mix}. Detailed experimental conditions for the individual NMR spectra are presented in the figure captions. For ^1H MAS, ^1H-^1H exchange, and $^{13}C\{^1H\}$ and $^{29}Si\{^1H\}$ HETCOR NMR experiments, the samples were dehydrated in vacuum at 100 °C for at least 12 h before NMR measurements. The sample was tightly packed into the rotor in a glovebox under a dry nitrogen atmosphere to avoid rehydration.

Other Characterization. Powder X-ray diffraction (XRD) patterns were collected on Wiggler-A beamline ($\lambda = 0.133320$ nm) at the National Synchrotron Radiation Research Center in Taiwan. Nitrogen adsorption–desorption isotherms were measured at 77 K on a Micromeritics ASAP 2020 analyzer. The sample was degassed at 180 °C for 3 h before measurements. BET (Brunauer–Emmett–Teller) areas were calculated from data in the relative pressure range of $P/P_0 = 0.05$–0.3. The pore size distribution was analyzed on the basis of the NLDFT (nonlocal density functional theory) model for spherical cavities from the adsorption branch.[41] Pore volumes excluding the effect of large interparticle void were determined from t-plot. Thermogravimetric analysis (TGA) was carried out on a Perkin-Elmer TGA7 thermogravimetric analyzer with a heating rate of 10 °C/min under air flow.

Results and Discussion

Structural Ordering as a Function of Phenyl Loading. The powder XRD patterns of the as-synthesized and template-extracted A-Ph-MB/*x* samples are shown in

(38) Huh, S.; Wiench, J. W.; Yoo, J.-C.; Pruski, M.; Lin, V. S. -Y. *Chem. Mater.* **2003**, *15*, 4247.
(39) *PEAKFIT* software, version 4.11; SYSTAT software Inc.: San Jose, CA, 1990–2002.
(40) Schmidt-Rohr, K.; Spiess, H. W. *Multidimensional Solid State NMR and Polymers*; Academic Press: New York, 1994; p 478.
(41) Ravikovitch, P. I.; Neimark, A. V. *Langmuir* **2002**, *18*, 1550.

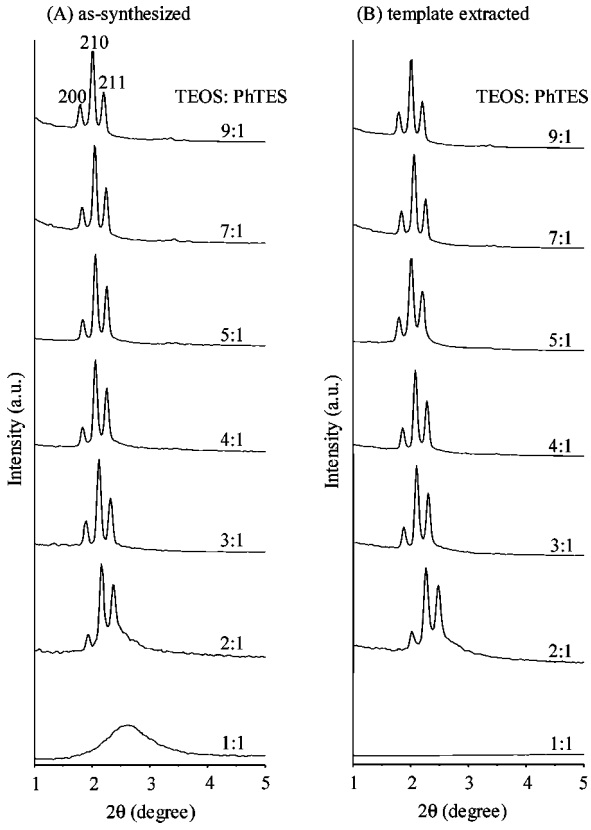

Figure 1. Powder XRD patterns of (A) as-synthesized and (B) template-extracted A-Ph-MB/*x* samples, synthesized with various TEOS:PhTES ratios.

Figure 1. All the as-synthesized samples showed three well-resolved XRD diffraction peaks in the region of 2θ = 1.5–2.5°, which can be indexed to the (200), (210), and (211) diffractions, characteristic of the cubic *Pm*3*n* mesostructure. This indicates that the presence of PhTES contents up to 33 mol % (based on silicon) in the initial synthesis mixture did not disrupt the structural ordering of SBA-1. After treatment with the ethanol/HCl mixture for template removal, these samples still preserved the structural order of their cubic mesostructures since there was no significant change in the XRD patterns. The positions of the reflections shifted slightly after the template was removed, indicating that there was little shrinkage of the cell dimensions of the materials. This result suggested that these phenyl-functionalized SBA-1 materials were stable toward the solvent extraction treatment. The structure order became significantly degraded for the as-synthesized sample with a high phenyl loading of 50 mol % (i.e., TEOS:PhTES = 1:1) since only a broad XRD diffraction peak was observed. Its structure was collapsed after template removal. For the mesoporous silicas MCM-41, HMS, and MCM-48 functionalized with phenyl groups, the maximum phenyl loading that can be incorporated into the mesoporous framework was only around 20, 10, and 7.5%, respectively.[2,14,42]

Thermal Stability and Textural Properties. The thermal stability of the phenyl functional groups within the mesoporous samples was determined by thermogravimetric analysis (TGA). The TGA curves of the selected as-synthesized and template-extracted samples are illustrated in Figure 2. Both products showed two main weight-loss regions. The small weight loss below 200 °C was due to the removal of physisorbed water and/or residual ethanol used in the solvent extraction process. The weight-loss curves of the as-synthesized materials were dominated by the relatively large loss at 200–300 °C caused by the decomposition of the surfactant CTMABr as it disappeared upon solvent extraction. On the other hand, some decomposition in the range of 500–600 °C, as evident from the peak at around 570 °C in the DTA curves (bottom, Figure 2), was observed for both as-synthesized and template-extracted A-Ph-MB/2 and A-Ph-MB/4 samples. This weight loss is mostly due to the decomposition of the phenyl functional groups anchored to the mesopore wall, indicative of the high thermal stability of Si−Ph bonds.

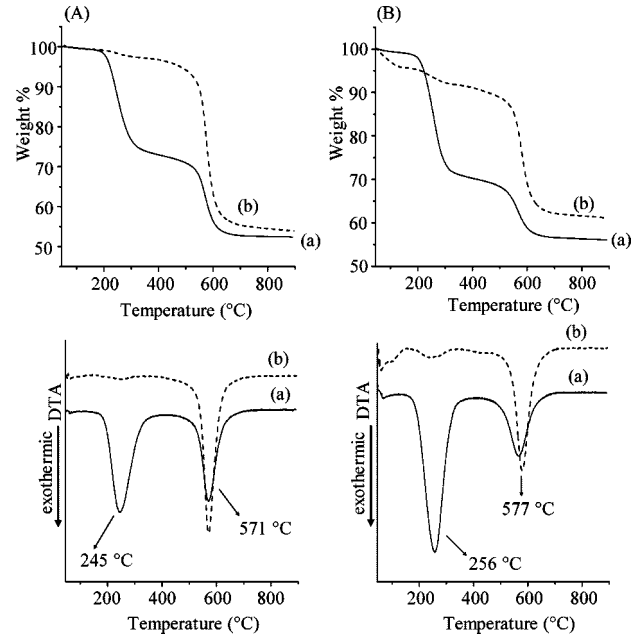

Figure 2. TGA (top) and DTA (bottom) curves of (A) A-Ph-MB/2 and (B) A-Ph-MB/4 samples (a) before and (b) after template extraction.

Nitrogen adsorption–desorption isotherms of the template-extracted A-Ph-MB/*x* samples, as well as the calculated pore size distribution, are shown in Figure 3. The results are also summarized in Table 1. All the isotherms were reversible, as typically observed for high quality SBA-1.[19–21] The isotherms changed from type IV for pure silica SBA-1 to type I for phenyl-functionalized SBA-1. An inflection point was observed at $P/P_0 \sim 0.85$ with low PhTES loadings (x = 9 and 7), which is most likely due to the increasing thickness of the adsorbed layer at the outer surface of the SBA-1 particles. For the samples with more PhTES incorporated, the particle size increased, and thus the contribution of the particle outer surface became less important. Both the mesopore volume and the BET surface area progressively decreased with increasing PhTES contents. Clearly, this can be attributed to the progressive filling of the mesopores with phenyl groups. Nevertheless, as demonstrated by the calculated pore size distribution, the filling was not uniform across all cavities.

The pore size was calculated from the isotherms according to the density function theory for spherical cavities.[41] For

(42) Hall, S. R.; Fowler, C. E.; Lebeau, B.; Mann, S. *Chem. Commun.* **1999**, 201.

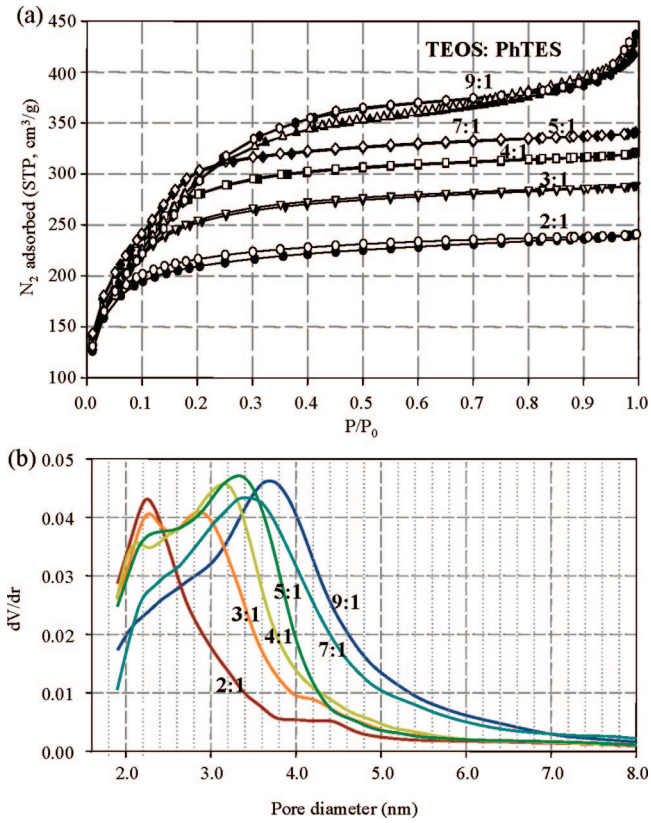

Figure 3. (a) N_2 adsorption–desorption isotherms and (b) pore size distribution curves of template-extracted A-Ph-MB/*x* samples, synthesized with various TEOS:PhTES ratios. The branches of the adsorption and desorption isotherms are presented by closed and open symbols, respectively.

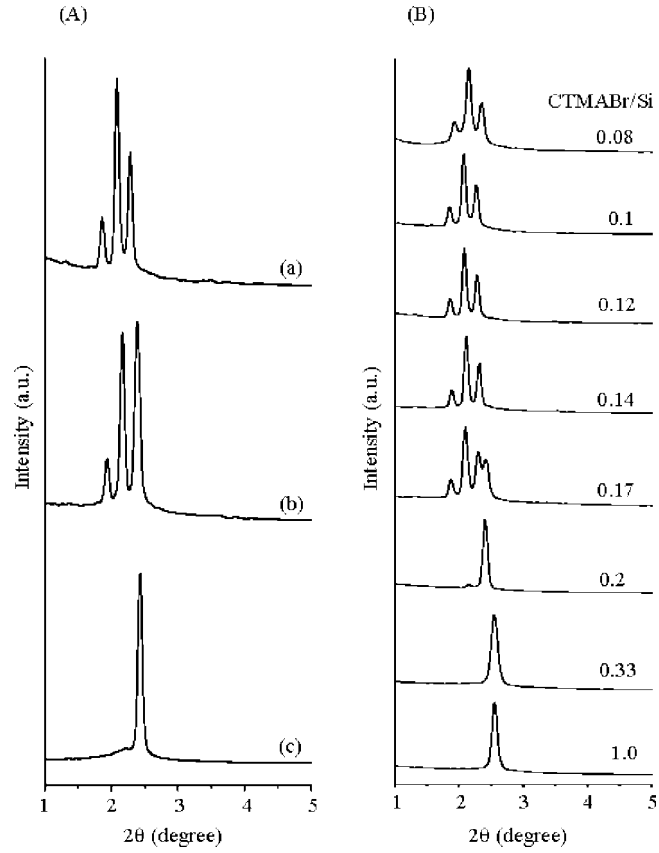

Figure 4. Powder XRD patterns of template-extracted A-Ph-MB/4 samples (A) synthesized with various synthesis temperatures: (a) 0, (b) 25, and (c) 50 °C (CTMABr/Si = 0.12) and (B) synthesized with various CTMABr/Si ratios. The silicon content includes TEOS and PhTES with a ratio of 4:1.

Table 1. Textural Properties of A-Ph-MB/*x* Samples after Template Extraction

TEOS:PhTES	d_{210} (nm)	a_0[a] (nm)	BET area (m^2/g)	pore volume (cm^3/g)	pore size (nm)	
9:1	3.82	8.5	1000	0.56		3.7
7:1	3.71	8.3	1000	0.58	2.2	3.5
5:1	3.82	8.5	990	0.52	2.2	3.4
4:1	3.67	8.2	920	0.49	2.2	3.2
3:1	3.64	8.1	820	0.44	2.2	2.8
2:1	3.71	8.3	660	0.36	2.2	

[a] Lattice parameters a_0 were calculated on the basis of the formula $a_0 = (\sqrt{5})d_{210}$.

uniform sized spherical cavities, the density function theory predicts a discontinuous capillary condensation step. The primary cause for the smooth and rounded isotherm is the cavity distribution in the material, although the finite size effect of the narrow pore and the roughness of the pore surface may all contribute to the smoothness. We have neglected the influence of the finite size effects or the surface roughness and attributed the finite slope of the isotherm to the pore size distribution effect.

At low phenyl loading ($x = 9$), a monomodal pore size distribution centered at about 3.7 nm was observed, which is similar to the case of pure silica SBA-1 without phenyl groups.[21,22] With progressive increase of the phenyl loadings, a new size population centered at about 2.2 nm started to immerge and the pore size distribution became bimodal at higher phenyl loadings. The weighting of the 2.2 nm population increased with increasing phenyl loadings and became dominant when the phenyl content was increased up to $x = 2$. In comparison with the case of pure silica SBA-1 without phenyl groups, the evolution of the pore size distribution suggests that the 2.2 nm cavities are those covered with phenyl groups, while the larger 3.7 nm cavities are those without phenyl groups. This implies that the incorporated phenyl groups prefer to cluster together during the synthesis and appear in the same cavity after the removal of surfactant.

Effect of Synthesis Temperature. The kinetics of the hydrolysis of TEOS and PhTES followed by their co-condensation is highly dependent on temperature. Therefore, the assembly temperature of the reaction system should play a key role in determining the final forms of the mesoporous materials. This is particularly true for the synthesis of SBA-1. In a previous study, Kim and Ryoo[19] have found that SBA-1 was favorably formed at low temperatures such as 0 °C, while it underwent undesirable phase transformation when the synthesis temperature was higher than 45 °C. To determine the effect of the synthesis temperature on the mesostructure of the phenyl-functionalized SBA-1, the assembly reactions were carried out at higher synthesis temperatures such as 25 and 50 °C for comparison.

Figure 4A shows the XRD patterns of template-extracted A-Ph-MB/4 samples, synthesized at different synthesis temperatures. When the synthesis temperature was raised to 25 °C, mixed phases consisting of cubic and hexagonal mesophases were observed, since the intensity of the (211)

diffraction peak was comparable to that of (210). Upon increasing the synthesis temperature up to 50 °C, a hexagonal phase was observed. This is consistent to the synthesis of pure silica SBA-1 at synthesis temperatures higher than 45 °C, at which a phase transformation from cubic SBA-1 mesophase to hexagonal SBA-3 mesophase occurs.

The effect of the assembly temperature on the formation of the mesostructure can be understood by considering the surfactant packing parameter g of the surfactant CTMABr with hydrophobic tails and hydrophilic headgroups. The surfactant packing parameter g is given by $g = V/(a_0 l)$, where V is the total volume of the surfactant chain, a_0 is the effective headgroup area at the organic–inorganic interface, and l is the surfactant chain length. As the assembly temperature of the mixture gel is raised, the conformational disorder due to the surfactant tail motion increases the effective surfactant volume, leading to a corresponding increase in the g value. At the same time, the repulsion of the charged headgroups of $CTMA^+$ is also increased with increasing temperature, which leads to an increase in the headgroup area a_0 value. These two antagonistic effects compete and direct the final forms of the mesostructure. In the present case, the former is predominant over the latter because a phase transformation associated with a greater g value ($>1/3$) was observed when the mesoporous silica was assembled at high temperatures.

In our recent studies,[21,43] we have demonstrated that addition of short-chain alcohols (methanol, ethanol) or polyols like D-fructose into the surfactant CTEABr solution can effectively prevent the uncontrollable phase transformation of SBA-1 even at high synthesis temperatures. The preservation of the cubic SBA-1 mesostructures, templated by a smaller headgroup surfactant CTMABr, in the presence of PhTES as another silicon source, is an interesting problem. It should be noted that a hexagonal SBA-3 mesophase, instead of cubic SBA-1, is often formed under such conditions. The special effect induced by PhTES must result in an enlargement of the effective headgroup area (a_0), possibly due to some specific interactions between the phenyl groups and the headgroups of the surfactant molecules, which maintains the g value in favor of the formation of cubic SBA-1 phase. As a result, no phase transformation of SBA-1 mesostructures was observed at low synthesis temperatures in the presence of PhTES. In contrast, the effect of the increased volume induced by increasing temperature cannot be balanced anymore and thus phase transformation to a hexagonal mesophase was observed with a higher synthesis temperature (50 °C).

Changes in the Composition and Type of Surfactant. Because the self-assembling capability of the surfactant depends on the surfactant concentration, a fine control on the concentration of the surfactant is essentially important for preparing highly ordered mesoporous materials. Figure 4B shows the XRD patterns of the A-Ph-MB/4 materials obtained by varying the CTMABr/Si ratio. When the CTMABr/Si ratio is in the range of 0.08 to 0.14, a cubic *Pm3n* mesophase was formed. Except for the patterns of the cubic mesophase, an additional diffraction peak was observed at a higher angle for the material prepared with a CTMABr/Si ratio of 0.17, indicating the formation of mixed phases. A hexagonal mesophase was formed when the CTMABr/Si ratio was greater than 0.2. Clearly, the formation of either cubic or hexagonal mesophases highly depends on the surfactant/Si ratios.

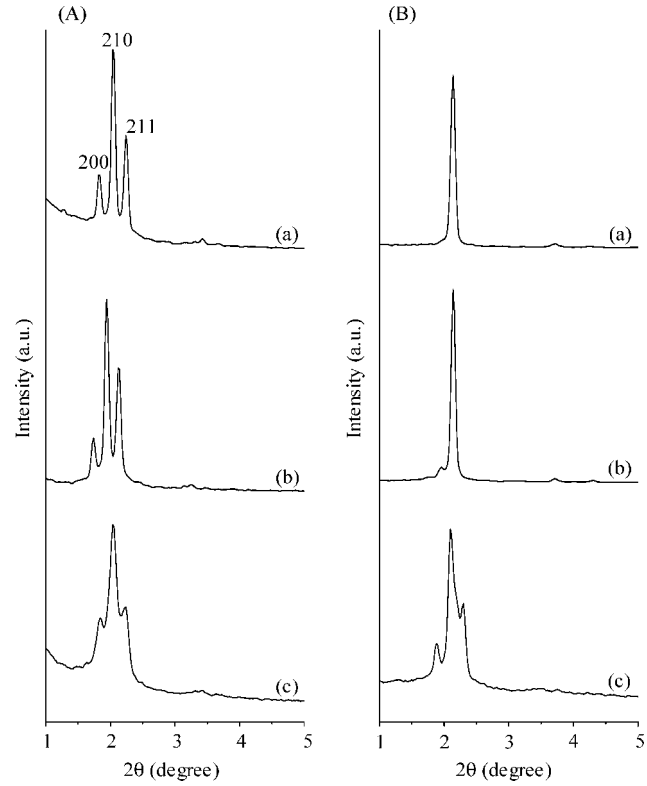

Figure 5. Powder XRD patterns of (A) as-synthesized samples, synthesized by method A and (B) synthesized by method B, templated by (a) CTMABr, (b) CTMACl, and (c) CTEABr, respectively, and with a TEOS:PhTES ratio of 7:1.

Figure 5 shows the XRD patterns of the materials templated by different surfactants with different compositions after template removal. All the materials, synthesized by method A, exhibit well-ordered cubic *Pm3n* structures by using CTMABr, CTMACl, and CTEABr as the surfactants. By using method B, on the other hand, only the material templated by CTEABr exhibited the *Pm3n* mesophase, while both the materials templated by CTMABr and CTMACl exhibited hexagonal mesophases. For the latter cases, the hexagonal mesophases were obtained when a surfactant/Si ratio of 0.2 was employed in both methods (see Figure 4B). Clearly, the surfactant/Si ratio plays an important role in governing the final forms of the mesostructures. When the surfactant/Si ratio changed from 0.12 to 0.2, a cubic mesophase was still obtained with CTEABr as the template, suggesting that the synthesis window for SBA-1 is larger by using the large headgroup surfactant CTEABr.

Multinuclear NMR Characterization. ^{13}C CPMAS NMR spectra confirm the presence of organic functional groups in the silica framework and indicate the efficiency of the template extraction procedure. Figure 6 shows the ^{13}C CPMAS NMR spectra of the as-synthesized and template-extracted A-Ph-MB/x samples as a function of phenyl loadings. The spectra of the as-synthesized samples exhibit

(43) Kao, H.-M.; Cheng, C.-C.; Ting, C.-C.; Hwang, L.-Y. *J. Mater. Chem.* **2005**, *15*, 2989.

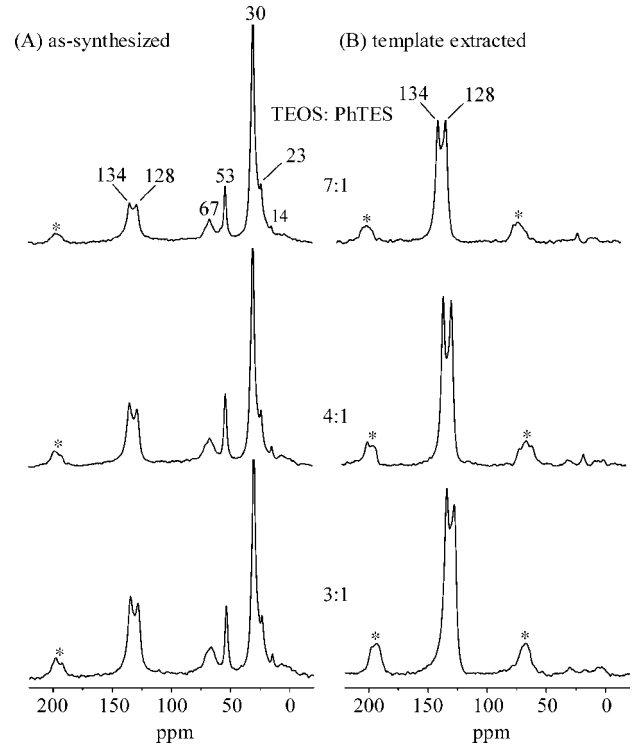

Figure 6. ^{13}C CPMAS NMR spectra of (A) as-synthesized and (B) template-extracted A-Ph-MB/*x*, synthesized with various TEOS:PhTES ratios, acquired at a spinning speed of 8 kHz. Asterisks denote spinning sidebands. For the spectra presented in part A, the intensity of the peak at 30 ppm is normalized for comparison. The peak at 67 ppm was partially overlapped with the spinning sideband from the peaks at 128 and 134 ppm.

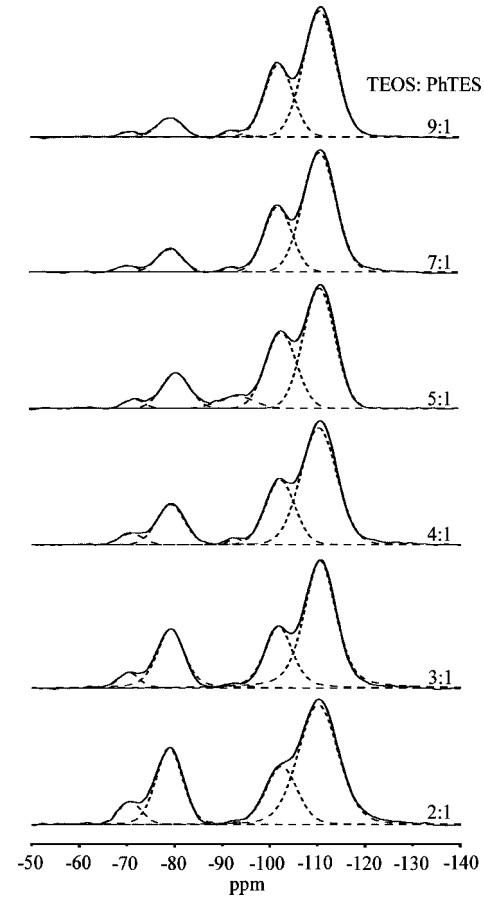

Figure 7. ^{29}Si MAS NMR spectra of template-extracted A-Ph-MB/*x*, synthesized with various TEOS:PhTES ratios. The dashed lines represent the components used for the spectral deconvolution.

the peaks at 14, 23, 30, 53, and 67 ppm, characteristic of the surfactant chains, and the peaks at 128 and 134 ppm are due to the phenyl groups incorporated. The peaks at 14, 23, and 30 ppm are due to the methylene carbons of the surfactant chain. The peak at 67 ppm is attributed to the α-carbon atoms adjacent to the surfactant headgroup on the alkyl chain (i.e., $-\mathbf{C}H_2-N-(CH_3)_3$), while the peak at 53 ppm is ascribed to the methyl groups of the surfactant headgroup (i.e., $-CH_2-N-(\mathbf{C}H_3)_3$). As seen in Figure 6A, the intensities of the peaks at 128 and 134 ppm due to the phenyl groups are proportional to the amounts of the phenyl groups incorporated, assuming that the peak intensity at 30 ppm due to the surfactant is constant for each as-synthesized sample. The main signal (30 ppm) of the residual surfactant CTMABr was not directly observed in the template-extracted sample, indicative of high efficiency of surfactant removal (Figure 6B). The observation of the phenyl peaks indicates that the integrity of this organic fragment is preserved upon surfactant removal.

^{29}Si MAS NMR was performed to provide a quantitative measure of the relative concentrations of Q^n and T^m functionalities. Five signals at around −92, −101, and −110 ppm, corresponding to Q^2 ($Si(OSi)_2(OH)_2$), Q^3 ($Si(OSi)_3(OH)$), and Q^4 ($Si(OSi)_4$) species, and −79 and −68 ppm, corresponding to T^3 ($RSi(OSi)_3$ and T^2 ($RSi(OSi)_2(OH)$) sites, respectively, where R is referred to phenyl group, were observed for the template-extracted samples (Figure 7). The observation of T groups indicates the presence of organosilane groups in the materials. The intensity of T groups increases as the concentration of PhTES in the initial composition is increased, indicating that the incorporated phenyl functional groups in the mesoporous silica materials is proportional to the PhTES contents added into the synthesis mixture. On the basis of distinct T^3 and T^2 signals in the ^{29}Si MAS NMR spectra of all samples, the relative integrated intensities of Q^n and T^m NMR signals allows the quantitative assessment of the incorporation degree of the organic moiety. As seen in Table 2, the ratios of $T^m/(T^m + Q^n)$ are in close agreement with those expected based on the composition of the initial mixture. This suggests that both TEOS and PhTES translate into the SBA-1 framework quite quantitatively.

Table 2. Relative Intensities of T^m and Q^n Groups Obtained from the ^{29}Si MAS NMR Spectra for the Template-Extracted A-Ph-MB/*x* Samples, where x Represents the TEOS/PhTES Ratio

TEOS:PhTES	T^2 (%)[a]	T^3 (%)	Q^2 (%)	Q^3 (%)	Q^4 (%)	$T^m/(T^m + Q^n)$
9:1	1.6	7.2	1.6	30.0	59.6	0.09
7:1	1.8	8.9	0.7	28.7	59.9	0.11
5:1	2.3	12.7	5.7	30.3	49.0	0.15
4:1	3.5	14.7	1.2	25.2	55.4	0.18
3:1	4.1	20.5	1.5	22.0	51.9	0.25
2:1	5.8	23.1	0.4	19.9	50.8	0.29

[a] The uncertainty is ±5%.

It is interesting to compare the ^{29}Si CPMAS NMR spectra acquired for the samples before and after surfactant removal. The intensity ratio changed from 0.90 to 0.43 for Q^4/Q^3 and 2.6 to 1.2 for T^3/T^2 upon surfactant removal (Figure S1, Supporting Information). The chief source of the magnetization transfer for the Q^4 species in the as-synthesized sample

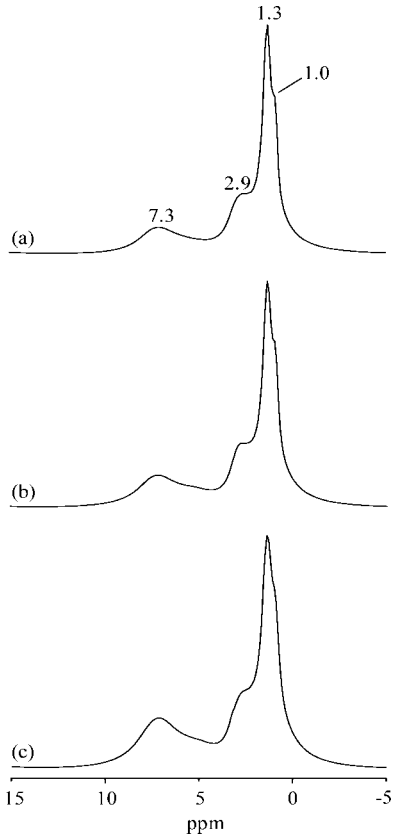

Figure 8. ^{1}H MAS NMR spectra of as-synthesized A-Ph-MB/*x*, acquired at a spinning speed of 8 kHz, where *x* = (a) 4, (b) 3, and (c) 2. The peak at 1.3 ppm due to the surfactant is normalized for comparison.

is the protons from the surfactant molecules. Besides the surfactant molecules, the Q^3 species also receive considerable magnetization transfer from the attached OH group. This enhances the CP signal intensity of the Q^3 species in the template-extracted sample, where the surfactant has been removed. The change in the intensity of the T^3 and T^2 units before and after surfactant removal is more complicated because both units contain protons from the OH groups and the phenyl groups. Nevertheless, the present ^{29}Si CPMAS NMR results show that the surfactant protons are less important for the build-up of the Q^3 signal than for the build-up of the Q^4 signal.

Attributing ^{1}H resonances in solid-state NMR spectra to particular chemical species is often difficult, because the narrow proton chemical shift range and strong homonuclear ^{1}H-^{1}H dipolar couplings cause ^{1}H NMR peaks to be often overlapping and broad, resulting in poor resolution in the spectrum. Figure 8 shows the ^{1}H MAS NMR spectra of the as-synthesized A-Ph-MB/*x* samples. Sufficient molecular mobilities and/or internuclear separations apparently exist for CTMABr at room temperature to produce relatively weak dipolar couplings between ^{1}H nuclei, so that resolved ^{1}H MAS spectra are obtained for the different samples. As a result, multiple-pulse homonuclear decoupling strategies are not required to resolve individual components in the ^{1}H MAS spectra for protonated species in the materials under investigation here. The ^{1}H MAS NMR spectra show three main peaks at 1.0, 1.3, and 2.9 ppm, respectively, attributed to alkyl chain CH_3 protons, alkyl chain CH_2 protons (exception made for $N-CH_2$ in the α-position), and $-CH_2-N-(CH_3)_3$ protons.[34b,44,45] Similar results were reported earlier in mesoporous silicas.[26,28,30] One exception is the small upfield shift of the $-CH_2-N-(CH_3)_3$ protons in the surfactant molecules, which often appear at around 3.1 ppm in most other mesoporous silicas.[26,28,30] The upfield shift of the $-CH_2-N-(CH_3)_3$ protons in the surfactant molecules in the present study could be related to the ring current effects from the nearby phenyl groups. This could be a good indicator for the spatial proximity between the surfactant and the phenyl groups and was confirmed by the ^{13}C{^{1}H} HETCOR NMR experiments as shown below. One additional peak of lower intensity was detected at around 7.3 ppm for phenyl groups, whose intensities were proportional to the phenyl loadings.

Silica−Surfactant Interfaces. ^{13}C{^{1}H} and ^{29}Si{^{1}H} HETCOR NMR of As-Synthesized Materials. With the ^{1}H NMR peaks identified in Figure 8, it is possible to correlate these resonances with those of nearby ^{13}C or ^{29}Si species through their respective ^{1}H-^{13}C or ^{1}H-^{29}Si dipolar couplings. Two-dimensional ^{13}C{^{1}H} HETCOR experiments were first used to correlate well-known ^{13}C NMR resonances from specific organic moieties to their corresponding ^{1}H NMR peaks to explore the exact location of these phenyl groups with respect to the surfactant molecules. As the $CTMA^+$ species and phenyl groups are the sole organic agents present in the present materials, all observed ^{1}H-^{13}C correlations arise from the structure-directing surfactant species and the phenyl functional groups. Thus, ^{13}C{^{1}H} HETCOR NMR is an ideal tool to correlate the ^{1}H peak positions with the ^{13}C peaks associated with the well-established carbon sites of the cationic $CTMA^+$ molecules and the phenyl functional groups pendant in the pore wall. As demonstrated in the previous study, the presence of water has a dominant effect on the ^{1}H NMR spectra of the mesoporous materials.[26,28,30] To avoid the complicated situation caused by the adsorbed water, samples were dehydrated under vacuum at 100 °C for at least 12 h prior to these NMR experiments to minimize the effects of the adsorbed water and to allow the chemical shifts for the ^{1}H peaks to be more accurately measured in these materials. 2D ^{13}C{^{1}H} HETCOR NMR experiments were recorded with different contact times (t_{CP} = 0.5, 1, and 5 ms), during which the magnetization transfer occurs between the ^{1}H and the ^{13}C spin systems, to probe the increasing internuclear distances and therefore to provide the information about through-space proximities between ^{1}H and ^{13}C sites (Figure 9). In the contour plot of the 2D ^{13}C{^{1}H} HETCOR NMR spectrum of A-Ph-MB/4, as shown in Figure 9a, the intensity profile shows clearly that, for a short contact time of 0.5 ms, the ^{1}H peak at 7.3 ppm is correlated to the phenyl carbons at 128 and 134 ppm (correlation peak A). The ^{13}C chemical shifts for the alkyl chain methylene carbons appear in the range from 14 to 30 ppm, and these correlate with their proton resonance at 1.3 ppm, while the carbon resonance at 53 ppm is associated with the terminal methyl group on

(44) Alonso, B.; Harris, R. K.; Kenwright, A. M. *J. Colloid Interface Sci.* **2002**, *251*, 366.
(45) Firouzi, A.; Schaefer, D. J.; Tolbert, S. H.; Stucky, G. D.; Chmelka, B. F. *J. Am. Chem. Soc.* **1997**, *119*, 9466.

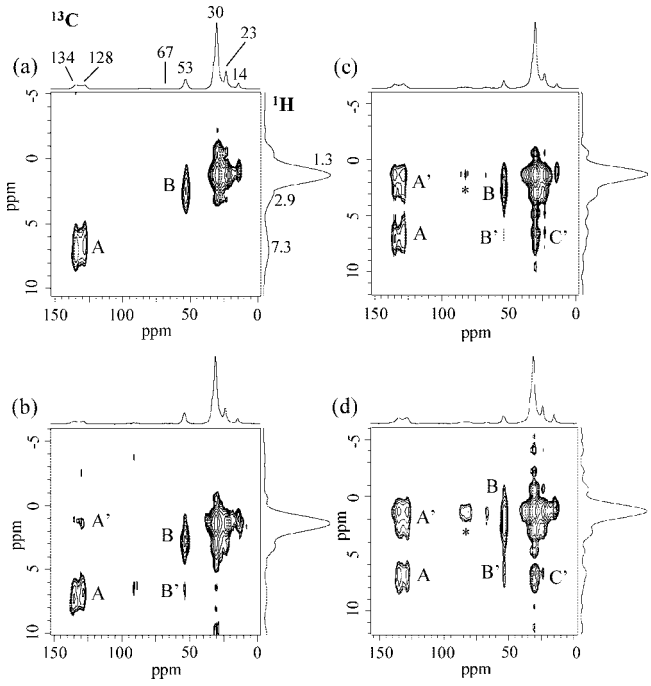

Figure 9. Two-dimensional ^{13}C{^{1}H} HETCOR NMR spectra recorded on as-synthesized A-Ph-MB/4 with different contact times: (a) 0.5, (b) 1 ms, and (c) 5 ms, and (d) on as-synthesized A-Ph-MB/3 with a contact time of 5 ms. All spectra were acquired at a spinning speed of 6 kHz, except at 5 kHz for (b). Asterisks denote spinning sidebands. The 1D projections are shown in skyline mode.

the surfactant tails and is correlated to the proton species at 2.9 and 1.3 ppm (correlation peak B). It should be noted that the only carbon species that are not observed in the ^{13}C dimension are the α-carbon atoms adjacent to the surfactant headgroup on the alkyl chain. The ^{13}C peak intensity for this site at 67 ppm is much weaker and broader than the other carbon species. The absence of this peak in the HETCOR NMR experiment is related to poor sensitivity of the experiment to detect minor species. No correlation peak between the phenyl groups and the surfactant molecules was observed at such a short contact time. With a longer contact time of 1 and 5 ms (Figure 9b,c), on the other hand, the only remarkable feature is that the intensity of the correlation peak A′ increases, and the ^{1}H peak at 7.3 ppm is now better correlated to both the trimethylammonium ^{13}C peaks at 53 ppm and the methylene carbons in the surfactant chain at 30 ppm in the ^{13}C dimension (B′ and C′). This observation provides clear evidence of the proximity of the headgroup in CTMABr to the pendant phenyl functional groups in the pore wall. As for the case of A-Ph-MB/3 with a higher loading of phenyl groups, these correlation peaks become more evident at a longer contact time of 5 ms (Figure 9d). The observation of correlation peaks at the contact times employed suggests that the phenyl groups are within ca. 1.0 nm dipole–dipole coupling distances to the protons on the headgroups of the structure-directing surfactant molecules.[26–30] Such a close proximity supports that there are some specific interactions between the surfactant polar headgroups and the phenyl groups.

^{13}C{^{1}H} HETCOR experiments were also recorded with ^{1}H PMLG (phase-modulated Lee−Goldburg) homonuclear

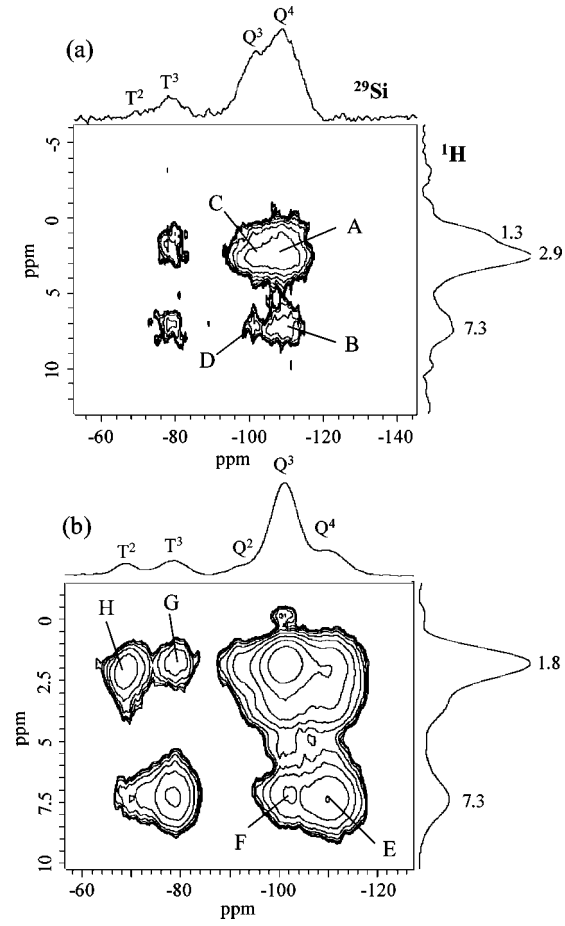

Figure 10. Two-dimensional ^{29}Si{^{1}H} HETCOR NMR spectra of (a) as-synthesized and (b) template-extracted A-Ph-MB/4, acquired with a contact time of 1 ms and at a spinning speed of 5 kHz. The 1D projections are shown in skyline mode.

decoupling during the t_1 evolution time.[46] The use of ^{1}H pulses under Lee−Goldburg conditions eliminates the ^{1}H-^{1}H homonuclear dipolar interactions and effectively prevents most of the ^{1}H spin diffusion process from taking place. The intensities of the correlation peaks between the proton signal of phenyl groups at 7.3 ppm and the carbon signals of the surfactant molecules at 53 ppm become more evident (see Figure S2, Supporting Information), which suggests that for a contact time of 5 ms, spin diffusion might occur between the protons of the phenyl groups and the large reservoir of protons from the surfactant molecules. This observation can be confirmed later by 2D ^{1}H-^{1}H homonuclear correlation experiments.

The ^{13}C{^{1}H} HETCOR NMR results are also corroborated by the ^{29}Si{^{1}H} HETCOR NMR spectrum shown in Figure 10a for the same as-synthesized A-Ph-MB/4 sample. Correlated peak intensities between ^{1}H and ^{29}Si resonances indicate close spatial proximities of the dipole–dipole coupled ^{1}H and ^{29}Si species; namely, that the T and Q ^{29}Si species of the silicate network are in close spatial proximity to the

(46) (a) Van Rossum, B. J.; Förster, H.; De Groot, H. J. M. *J. Magn. Reson.* **1997**, *124*, 516. (b) Vinagradov, E.; Madhu, P. K.; Vega, S. *Chem. Phys. Lett.* **1999**, *314*, 443. (c) Van Rossum, B. J.; De Groot, C. P.; Ladizhansky, V.; Vega, S.; De Groot, H. J. M. *J. Am. Chem. Soc.* **2000**, *122*, 3465. (d) Sozzani, P.; Bracco, S.; Comotti, A.; Camurati, I.; Simonutti, R. *J. Am. Chem. Soc.* **2003**, *125*, 12881. (e) Sozzani, P.; Comotti, A.; Bracco, S.; Simonutti, R. *Chem. Commun.* **2004**, 768.

protons associated with the surfactant molecules. Both the protons from the headgroup methyl species of the surfactant molecules (^{1}H, δ = 2.9 ppm) and those from the phenyl groups (^{1}H, δ = 7.3 ppm) are correlated to the Q^4 and Q^3 ^{29}Si species in the silica framework (correlation peaks A−D in the figure). The presence of a weak correlation peak between the T species and the surfactant protons is the signature of a longer distance between those species and/or a lower concentration of phenyl groups. Thus, both ^{29}Si{^{1}H} and ^{13}C{^{1}H} HETCOR experiments prove unequivocally that the phenyl groups have been incorporated into the as-synthesized material, and those are in close proximities to the surfactant molecules.

Distribution of Organic Functional Groups. Following solvent extraction treatment for surfactant removal, the ^{29}Si{^{1}H} HETCOR NMR experiment was repeated to establish the successful incorporation of the phenyl groups into the silica framework and to demonstrate their distribution in the resulting mesoporous material. Figure 10b displays the contour plot of the 2D ^{29}Si{^{1}H} HETCOR NMR spectrum for the template-extracted A-Ph-MB/4 material. It is advantageous for such HETCOR NMR experiments with a short contact time of 1 ms to measure only correlations between spatially adjacent species. As shown in Figure 10b, it reveals that both the Q^3 and the Q^4 species are correlated strongly to the phenyl proton resonance at 7.3 ppm (correlation peaks E and F). Although the projection intensity of the Q^4 species is much weaker than that of the Q^3 species, a stronger correlation between the protons of the phenyl groups and the Q^4 species (correlation peak E) is observed, as compared to that of the Q^3 species (correlation peak F). The observation of such signal intensity in the contour plot reflects that the ^{1}H-^{29}Si dipolar couplings between the protons of the phenyl groups and the Q^4 species are larger, as compared to those between the phenyl groups and the Q^3 species, indicating that the T species are in closer proximity to Q^4 species than to Q^3 species in the template-extracted material. As expected, the ^{1}H peak at 1.8 ppm from the SiOH groups was predominantly correlated to the Q^3 species. Clear correlations were also observed between the T sites and the ^{1}H peak at 1.8 ppm (correlation peaks G and H). Since both the T^2 and Q^3 species contain SiOH groups, further discrimination for the proximity of the T^2 and T^3 groups to the Q^3 species is not feasible. On the basis of ^{29}Si{^{1}H} HETCOR NMR, a preferable distribution of the phenyl functional groups incorporated was established; that is, the T phenyl groups are in closer proximity to the Q^4 groups than to the Q^3 groups. This is of great importance because the distribution of the organic functional groups in the silica framework of mesoporous organosilicas is better understood. Moreover, the detection of the dipolar couplings between the ^{29}Si Q species and the protons associated with the phenyl moieties establishes that phenylsilanes are cross-linked to the mesoporous silica framework, instead of forming a separate phase. Therefore, the 2D ^{29}Si{^{1}H} HETCOR NMR experiments also provide direct molecular-level evidence for the co-condensation of PhTES and TEOS in the synthesis of mesoporous organosilicas. On the basis of the 2D ^{13}C{^{1}H} and ^{29}Si{^{1}H} HETCOR experiments, a schematic representation of the spatial arrangement of these silicon species in the silica framework and the surfactant molecules is given in Scheme 1. Such detailed structural information arises from the enhanced resolution provided by the 2D HETCOR experiment and reflects the utility of two-dimensional solid-state NMR techniques for correlating molecular proximities in these complicated heterogeneous systems.

Scheme 1. Schematic Representation of the Spatial Arrangement of the Surfactant Molecules and the Silicate Species in the Silica Framework[a]

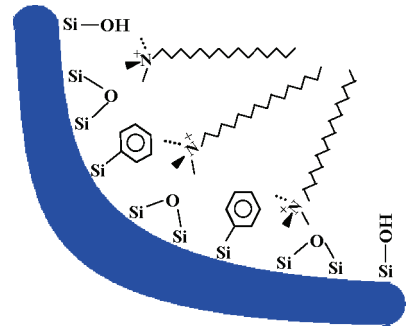

[a] The blue part represents the silica framework.

2D ^{1}H-^{1}H Homonuclear Correlation MAS NMR. Another way to probe the proximity between the phenyl groups and the surfactant is to record a 2D ^{1}H-^{1}H homonuclear correlation MAS NMR spectrum, to trace the ^{1}H magnetization transfer between different proton species in the material. This transfer is governed by spin diffusion that depends on dipole–dipole interactions among different proton species and thus the molecular distances between the protons. The diffusion of the proton magnetization during the mixing period, the time that the dipolar-coupled species are allowed to interact, can be regulated to probe the increasing internuclear distances, depending on the density of the coupled-proton system. Longer mixing times allow weaker ^{1}H-^{1}H couplings to be established. However, this kind of experiment requires high resolution ^{1}H NMR spectra to distinguish the various proton sources. The present phenyl functionalized SBA-1 sample is a good candidate because the ^{1}H chemical shifts of the protons of the phenyl groups and those in the surfactant molecules are well separated. Moreover, different portions of the surfactant give relatively good resolution of ^{1}H MAS NMR spectrum due to the high mobility of the surfactant.

2D ^{1}H-^{1}H homonuclear exchange experiments were performed on the as-synthesized A-Ph-MB/3 and A-Ph-MB/4 samples (Figure 11 and Figure S3 of Supporting Information) for different mixing times, during which magnetization transfer may occurs between the various protons. Cross-peaks were not visible for short mixing times (t_{mix} from 0 to 2 ms), indicating that the phenyl groups and the surfactant molecules can be considered to be isolated for this time scale. Cross-peaks between the peak at 7.3 and and that at 2.9 ppm started to be observed at a short mixing time of 3 ms for A-Ph-MB/3, while a longer mixing time of 5 ms was needed for A-Ph-MB/4. After 7 ms of polarization transfer, as shown in Figure 11b and Figure S3b, Supporting Information, a stronger cross-peak connecting the phenyl hydrogen at 7.3

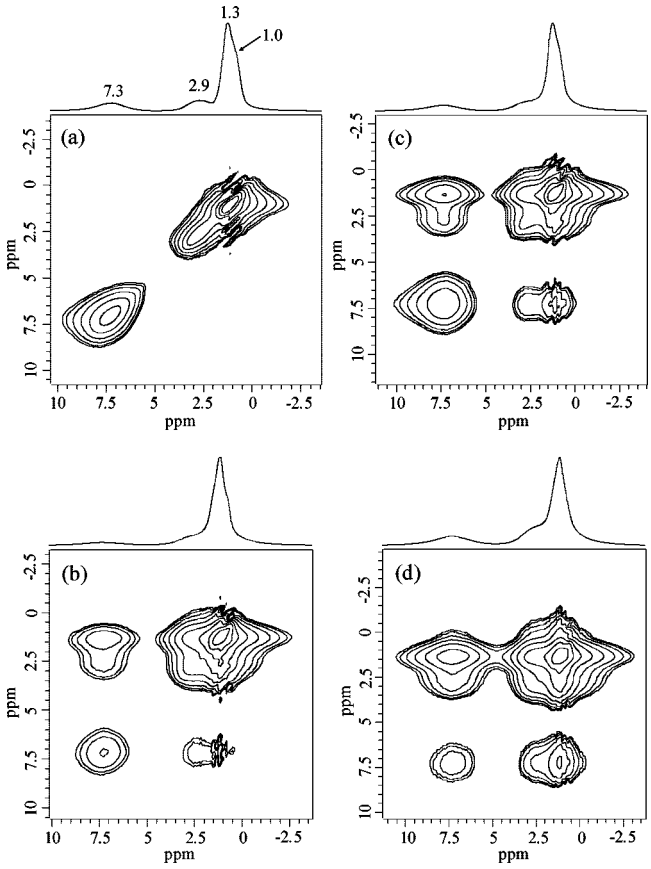

Figure 11. Two-dimensional ^{1}H-^{1}H exchange NMR spectra of as-synthesized A-Ph-MB/3 as a function of mixing time, t_{mix} = (a) 0.1, (b) 7, (c) 10, and (d) 20 ms, acquired with a spinning speed of 10 kHz.

ppm to the methyl headgroup hydrogens at 2.9 ppm was observed for A-Ph-MB/3, indicating that the magnetization exchange between these two sites is faster in A-Ph-MB/3 due to its higher density of phenyl groups. By increasing the mixing time, the magnetization was first transferred toward the protons of the headgroup of the surfactant and then progressively transferred to the protons of the aliphatic chains, that is, the interior of the surfactant micelle. It has been reported that a sufficient long carbon chain (at least three methylene units) in the functional group of the organosilane allows an interaction with the hydrophobic core of the structure-directing micelle, thereby permitting the successful incorporation of the organosilane into the pore walls of the mesostructure.[14] In fact, it has been reported that benzene molecules are preferably located at the hydrophilic−hydrophobic interface.[44] By combination of 2D ^{13}C{^{1}H}, ^{29}Si{^{1}H} heteronuclear, and ^{1}H-^{1}H homonuclear correlation NMR experiments, the presence of specific interactions between the incorporated phenyl groups and the surfactant polar headgroups can be identified unambiguously.

Conclusions

The phenyl functional groups up to 33 mol % were successfully introduced into the silica framework of cubic mesoporous silica SBA-1 via co-condensation of phenyltriethoxysilane and tetraethoxysilane under acidic conditions. The presence of pendant phenyl groups in the materials, along with detailed information on their interactions with the surfactant headgroups, was unambiguously established through the use of 2D ^{13}C{^{1}H} and ^{29}Si{^{1}H} HETCOR, ^{1}H-^{1}H exchange solid-state NMR studies. In particular, on the basis of ^{29}Si{^{1}H} HETCOR NMR performed on the template-extracted sample, a preferable distribution of the phenyl functional groups incorporated was established; that is, the phenyl groups are in closer proximity to the Q^4 groups than to the Q^3 groups.

Acknowledgment. The financial support of this work by the National Science Council of Taiwan is gratefully acknowledged.

Supporting Information Available: ^{29}Si MAS and CPMAS NMR spectra of as-synthesized and template-extracted A-Ph-MB/4 (Figure S1), 2D ^{13}C{^{1}H} PMLG-HETCOR NMR spectrum of A-Ph-MB/3 and A-Ph-MB/4 (Figure S2), and 2D ^{1}H-^{1}H exchange NMR spectra of A-Ph-MB/4 (Figure S3) (PDF). This material is available free of charge via the Internet at http://pubs.acs.org.

CM800147Z